Accurate, two-state ab initio study of the ground and first-excited states of He_2^+, including exact treatment of all Born–Oppenheimer correction terms

Junkai Xie, Bill Poirier, and Gregory I. Gellene

Citation: The Journal of Chemical Physics **122**, 184310 (2005); doi: 10.1063/1.1891685
View online: http://dx.doi.org/10.1063/1.1891685
View Table of Contents: http://aip.scitation.org/toc/jcp/122/18
Published by the American Institute of Physics

Accurate, two-state *ab initio* study of the ground and first-excited states of He_2^+, including exact treatment of all Born–Oppenheimer correction terms

Junkai Xie, Bill Poirier, and Gregory I. Gellene
Department of Chemistry and Biochemistry, Texas Tech University, Lubbock, Texas 79409-1061

(Received 19 July 2004; accepted 23 February 2005; published online 9 May 2005)

Born–Oppenheimer (BO) potentials for the ground and first-excited electronic states of He_2^+ are determined using high level *ab initio* techniques for internuclear separations R of 1.2–100 bohrs and accurately fit to analytical functions. In the present formulation, the BO potentials are nuclear mass independent, and the corresponding BO approximation is obtained by ignoring four terms of the full rovibronic Hamiltonian. These four Born–Oppenheimer correction (BOC) terms are as follows: (1) mass polarization, (2) electronic orbital angular momentum, (3) first derivative with respect to R, and (4) second derivative with respect to R. In order to enable an exact rovibronic calculation, each of the four BOC terms are computed as a function of R, for the two electronic states and for their coupling, without any approximation or use of empirical parameters. Each of the BOC terms is found to make a contribution to the total energy over at least some portion of the range of R investigated. Interestingly, the most significant coupling contribution arises from the electronic orbital angular momentum term, which is evidently computed for the first time in this work. Although several BOC curves exhibit a nontrivial dependence on R, all are accurately fit to analytical functions. The resulting functions, together with the BO potentials, are used to compute exact rovibronic energy levels for $^3He\ ^3He^+$, $^3He\ ^4He^+$, and $^4He\ ^4He^+$. Comparison to available high quality experimental data indicates that the present BOC potentials provide the most accurate representation currently available of both the low- and high-lying levels of the ground electronic state and the bound levels of the excited state. © *2005 American Institute of Physics*.
[DOI: 10.1063/1.1891685]

I. INTRODUCTION

The work of Born and Oppenheimer,[1] Born,[2] and Born and Huang,[3] which developed the foundation for separating the motion of light electrons from that of heavy nuclei, established the theory underlying adiabatic electronic processes that is the almost universal starting point for the consideration of molecular energetics and dynamics. At the simplest level of approximation, perhaps most accurately labeled the "Born–Oppenheimer expansion adiabatic approximation",[4] but in general practice referred to as simply the "Born–Oppenheimer approximation" (BO),[5,6] the nonrelativistic Schrödinger equation for electron motion in the field of fixed nuclei is solved repeatedly for various nuclear positions to generate a potential energy surface (PES) that governs the motion of the nuclei. A nuclear motion Schrödinger equation containing this PES is then solved to determine information about bound rovibration levels and/or quantum dynamical processes in the continuum. In many cases, this level of approximation is sufficiently accurate to allow quantitative comparisons between theoretical and experimental results.

In the next level of approximation, known as the "Born method,"[2,4] the BO approximation is improved upon via a first-order perturbation theory consideration of some or all terms in the full rovibronic Hamiltonian that were ignored in the BO approximation [i.e., Born–Oppenheimer correction (BOC) terms[7]]. The calculations can be performed at a single representative nuclear geometry, or, with increased sophistication, as a function of nuclear geometry with the resulting PESs being mass (i.e., isotope) dependent. In the third and final level of calculation, the adiabatic or rovibration picture is abandoned altogether, in favor of a single rovibronic calculation that couples together multiple electronic states.

The present work applies these three levels of approximation to the determination of the bound rovibronic levels of the He_2^+ ion, involving the ground and first-excited electronic states. This system was chosen for four reasons. First, the relatively small number of electrons allows high level *ab initio* calculations of the two BO PESs to be performed.[8–15] Noteworthy in this regard are the recent results of Cencek and Rychlewski (CR),[8] and of Carrington, Pyne, and Knowles (CPK),[9] to which the present results will be compared. Second, Yu and Wing[16] have reported high-resolution infrared spectroscopy for the low rovibration levels of $^3He^4He^+$, and CPK [Ref. 9] have observed and assigned high-resolution electronic spectra for $^4He_2^+$ involving high rovibration levels of the $X^2\Sigma_u^+$ ground electronic state and several rovibration levels of the weakly bound $A^2\Sigma_g^+$ first-excited electronic state, to which comparisons can be made. Third, the BOC energetic contribution to the $He+He^+$ asymptotic dissociation limit has been well established by previous high-level atomic calculations.[17] Reproducing these results in both atomic and molecular based calculations pro-

vides a valuable check of the present methodology. And fourth, unusual symmetry induced kinetic isotope effects (SIKIEs) have been reported for He_2^+ formation[18] where the asymmetric $^3He^4He^+$ ion formation rate constant was found to be more than twice that for either symmetric ion, $^4He_2^+$ or $^3He_2^+$. (This enhancement is above and beyond the ordinary statistical factor of 2 due to the two entrance channels.) A recent theoretical study[19] has established that, under the experimental conditions of the SIKIE study, He_2^+ ion formation proceeds dominantly though the two-step, energy transfer mechanism:

$$He + He^+ \leftrightarrows (He_2^+)^*, \tag{1}$$

$$(He_2^+)^* + He \rightarrow He_2^+ + He. \tag{2}$$

Thus, a theoretical understanding of the SIKIEs in this system requires detailed information on the BOC coupling between the ground and first-excited electronic states, which can influence the $He+He^+$ collision dynamics involving distinguishable helium isotopes. However, the effect of BOC considerations on the dynamics of reaction (1) is beyond the scope of the present study and will be considered in a subsequent publication.

II. THEORY

A. Hamiltonian

We are interested in obtaining a first-principles derivation of the potentials and rovibronic levels of He_2^+, accurate to around 0.1 cm^{-1} or better. For this system at this level of accuracy, relativistic effects are not expected to play a significant role, nor are hyperfine interactions. Moreover, the electron spin-orbit interaction can be ignored, as only the lowest two $^2\Sigma^+$ electronic states are relevant (these lie about 18 000 cm^{-1} below the next lowest electronic states, which have Π character). The approximations described above are the *only* ones that will be applied in all subsequent analysis.

Following Bunker,[20] the diatomic He_2^+ rovibronic Hamiltonian is therefore given by

$$\hat{\boldsymbol{H}} = \hat{\boldsymbol{T}}_e + \hat{\boldsymbol{T}}_N + \hat{\boldsymbol{T}}_{\rm mp} + V(\vec{r}_i,\vec{R}), \tag{3}$$

for which the kinetic energy is the sum of electronic $\hat{\boldsymbol{T}}_e$, nuclear $\hat{\boldsymbol{T}}_N$, and mass polarization $\hat{\boldsymbol{T}}_{\rm mp}$ contributions. These are given explicitly as follows:

$$\hat{\boldsymbol{T}}_e = -\frac{\hbar^2}{2m_e}\sum_{i=1}^{3}\nabla_i^2, \tag{4}$$

$$\hat{\boldsymbol{T}}_N = \hat{\boldsymbol{T}}_{\rm vib} + \hat{\boldsymbol{T}}_{\rm rot} = -\frac{\hbar^2}{2\mu}\frac{\partial^2}{\partial R^2} + \frac{\hat{\boldsymbol{R}}^2}{2\mu R^2}, \tag{5}$$

$$\hat{\boldsymbol{T}}_{\rm mp} = -\frac{\hbar^2}{2M}\sum_{i,j=1}^{3}\boldsymbol{\nabla}_i\cdot\boldsymbol{\nabla}_j, \tag{6}$$

where $M=m_A+m_B$ is the total nuclear mass, $\mu=m_Am_B/M$ is the nuclear reduced mass, and the Laplacians in Eqs. (4) and (6) are relative to the nuclear center of mass.

In Eq. (5) above, $\hat{\boldsymbol{R}}^2=\vec{\hat{\boldsymbol{R}}}\cdot\vec{\hat{\boldsymbol{R}}}$ is our designation for the total rovibration angular momentum operator, i.e.,

$$\hat{\boldsymbol{R}}^2 = -\hbar^2\left[\frac{1}{\sin^2\theta}\frac{\partial^2}{\partial\phi^2} + \frac{1}{\sin\theta}\frac{\partial}{\partial\theta}\left(\sin\theta\frac{\partial}{\partial\theta}\right)\right]. \tag{7}$$

In the present $^2\Sigma^+$ context, for which Hund's case (b) is anticipated (but not assumed as of yet), the relevant angular momentum is $\vec{\hat{\boldsymbol{N}}}=\vec{\hat{\boldsymbol{R}}}+\vec{\hat{\boldsymbol{L}}}$, the rovibronic angular momentum ($\vec{\hat{\boldsymbol{J}}}$ and $\vec{\hat{\boldsymbol{N}}}$ are not identical for the present system, because the total electron spin is not zero). The standard "trick"[21] is to replace $\vec{\hat{\boldsymbol{R}}}$ in Eq. (5) with $\vec{\hat{\boldsymbol{R}}}=\vec{\hat{\boldsymbol{N}}}-\vec{\hat{\boldsymbol{L}}}$, which in the body-fixed orientation[21–23] can then be treated using the conventional angular momentum machinery to yield

$$\hat{\boldsymbol{T}}_{\rm rot} = \frac{1}{2\mu R^2}[\vec{\hat{\boldsymbol{N}}}-\vec{\hat{\boldsymbol{L}}}]^2 = \frac{1}{2\mu R^2}[\hat{\boldsymbol{N}}^2+\hat{\boldsymbol{L}}^2-2\vec{\hat{\boldsymbol{N}}}\cdot\vec{\hat{\boldsymbol{L}}}]. \tag{8}$$

In principle, $\hat{\boldsymbol{T}}_{\rm rot}$ introduces angular momentum coupling through the last bracketed term in Eq. (8). However, this coupling is identically zero for the present $^2\Sigma^+$ electronic state restriction, thus implying that both N and M_N are good quantum numbers, i.e., Hund's case (b). The exact, N-dependent rovibronic Hamiltonian thus becomes

$$\hat{\boldsymbol{H}}^N = \hat{\boldsymbol{T}}_e + V(r,R) + \frac{N(N+1)}{2\mu R^2} + \hat{\boldsymbol{T}}_{\rm vib} + \hat{\boldsymbol{T}}_{\rm mp} + \frac{\hat{L}^2}{2\mu R^2}. \tag{9}$$

B. Born–Oppenheimer potentials

The first two terms on the right-hand side (RHS) of Eq. (9), for fixed nuclear separation R, are taken to constitute the electronic Hamiltonian $\hat{H}_e$. The eigenvalues of $\hat{H}_e$, as functions of R, constitute the BO potential energy curves. For the present He_2^+ application, the ground ($X\,^2\Sigma_u^+$) and first-excited ($A\,^2\Sigma_g^+$) electronic states were obtained via numerical solution of

$$\hat{\boldsymbol{T}}_e + V(r,R)\Phi_e^n(r;R) = V_e^n(R)\Phi_e^n(r;R). \tag{10}$$

Equation (10) was solved for 70 different values of R between 1.2 and 100 a.u. The index n refers to the particular electronic state and varies (in the present study) over the two values u and g, denoting ground and first-excited electronic states, respectively.

Numerical solutions to Eq. (10) were obtained using the suite of codes contained in the MOLPRO 2003.3 package.[24] These *ab initio* calculations used the sextuple ζ basis set,[9] d-aug-cc-pV6Z, consisting of $(10s5p4d3g2h1i)$ primitive functions contracted to $[6s5p4d3g2h1i]$ and augmented by an uncontracted $(2s2p2d2g2h2i)$ set of diffuse functions.[25] Pure spherical harmonic functions were used throughout. This basis set was used in complete active space multiconfigurational self-consistent-field (MCSCF) (Refs. 26 and 27) calculations, followed by internally contracted configuration interaction in the single and double space (MRCISD) (Refs. 28 and 29) with a Davidson correction[30] Q. In the MCSCF calculations the three valence electrons were distributed among the ten orbitals arising from the $1s$, $2s$, and $2p$

TABLE I. Comparison of calculated D_e and R_e values for the $X\,^2\Sigma_u^+$ and $A\,^2\Sigma_g^+$ states of He_2^+.

		BO				Modified Born		
State	Parameter	CPK	CPK′	CR	This work	$^3He\,^3He^+$	$^3He\,^4He^+$	$^4He\,^4He^+$
$X\,^2\Sigma_u^+$	$D_e(cm^{-1})$	19 943.56	19 969.37	19 945.98	19 945.82	19 945.90	19 940.98	19 945.82
	R_e(a.u.)	2.043	2.0430	2.042	2.042 39	2.042 99	2.042 98	2.042 99
$A\,^2\Sigma_g^+$	$D_e(cm^{-1})$	17.33			17.345 2	17.372 9	20.341 4	17.382 0
	R_e(a.u.)	8.750			8.741 9	8.746 9	8.651 0	8.748 5

atomic orbitals of each helium atom. Because MRCISD calculations are not size extensive, the energy of the separated atoms (V_e^∞), which is identical for the $X\,^2\Sigma_u^+$ and $A\,^2\Sigma_g^+$ states, was determined by a supermolecule calculation with $R=5\times10^4$ a.u.

Induction and dispersion forces control the long-range region of the He^+/He interaction of both potentials, and give rise to all of the attractive interaction in the excited electronic state. Calculated values for dipole (α_1) and quadrupole (α_2) polarizibilities and the dipole second hyperpolarizibility (γ) of He are 1.382 874, 2.444 14, and 42.8989 a.u., respectively. These results compare favorably with the best literature values[31–33] of 1.383 15, 2.4403, and 43.1 a.u., respectively, indicating that this part of the potential is being well described.

Analytical BO potential energy curves were developed by a nonlinear least squares fit of $V_e^u(R)-V_e^\infty$ to the function

$$U^u(R) = u_{er}(R)s_s(R) + u_l(R)s_l(R) \tag{11}$$

for the ground $X\,^2\Sigma_u^+$ state and $V_e^g(R)-V_e^\infty$ to the function

$$U^g(R) = u_{ex}(R) + u_l(R)s_l(R) \tag{12}$$

for the first-excited $A\,^2\Sigma_g^+$ state. In Eqs. (11) and (12), $u_l(R)$ is the long-range potential function given explicitly by

$$u_l(R) = -\frac{\alpha_1}{2R^4} - \frac{\alpha_2}{2R^6} - \frac{c_6}{R^6} - \frac{\alpha_3}{2R^8} - \frac{\gamma}{24R^8} - \frac{c_{81}}{R^8} - \frac{c_{82}}{R^8}, \tag{13}$$

where α_3 is the octopole polarizibility and c_6, c_{81}, and c_{82} are the multipolar dispersion coefficients. The calculated values for α_1, α_2, and γ were used without adjustment and α_3, c_6, c_{81}, and c_{82} were taken as their literature values[32,33] of 10.62, 0.3747, 1.845, and 0.867 a.u., respectively. Thus, $u_l(R)$ contains no adjustable parameters. The functions $s_s(R)$ and $s_l(R)$ are short- and long-range switching functions, respectively, given by

$$s_s(R) = 0.5[1 - \tanh[a_s(R-b_s)]], \tag{14}$$

$$s_l(R) = 0.5[1 + \tanh[a_l(R-b_l)]]. \tag{15}$$

Although the optimized values of a_l and b_l differ for $U^u(R)$ and $U^g(R)$, the use of identical $u_l(R)$ functions ensures the required asymptotic degeneracy of these two BO potentials as $R\to\infty$. The short-range interactions are described by an extended Rydberg-like function $u_{er}(R)$ for $U^u(R)$ and a biexponential repulsive function $u_{ex}(R)$ for $U^g(R)$, given by

$$u_{er}(R) = \sum_{i=0}^{8} a_i(R-R_0)^i e^{-b(R-R_e)}, \tag{16}$$

$$u_{ex}(R) = a_0\exp(-a_1R - a_2R^2) + b_0\exp(-b_1R - b_2R^2). \tag{17}$$

It might have been thought that because $u_{er}(R)\to0$ as $R\to\infty$, $s_s(R)$ would not be necessary. However, it was found that an $u_{er}(R)$ function that faithfully described $U^u(R)$ near the potential minimum was too attractive at intermediate values of R, and this problem was addressed by the inclusion of $s_s(R)$. Also, the MRCISD results were found to underestimate slightly the long-range interaction as given by Eq. (13); whereas, the MRCISD+Q results were in essentially quantitative agreement.

A total of 15 adjustable parameters [Table I of the associated Electronic Physics Auxiliary Publication Service[34] (EPAPS)] were used to fit the $U^u(R)$ potential with a rms error of 0.30×10^{-5} a.u. and a maximum error of 1.1×10^{-5} a.u. occurring at 1.5 bohrs. Alternatively, only 8 adjustable parameters (Table II of the associated EPAPS material[34]) were used to fit the $U^g(R)$ potential with a rms of 0.17×10^{-6} a.u. and a maximum error of 2.2×10^{-6} a.u. occurring at 6.5 bohrs. The two potentials are shown graphically in Fig. 1.

C. Born–Oppenheimer correction terms

With the present choice for the BO electronic Hamiltonian, four BOC terms can be identified, all of which are relevant to this study. The first two stem from the last two terms of Eq. (9), which are related, respectively, to mass polarization and to the electron orbital angular momentum. The last two terms arise from the action of $\hat{\boldsymbol{T}}_{\rm vib}$ on the electronic states $\Phi_e^n(r;R)$, which depend parametrically on R and correspond, respectively, to first and second derivatives with respect to R. (It is only these nuclear coordinate derivative terms that constitute BOCs in traditional treatments.) Associated with each of the BOC terms are a set of potential-like functions, denoted $\boldsymbol{w}_{\rm mp}(R), \boldsymbol{w}_l(R), \boldsymbol{w}_1(R)$, and $\boldsymbol{w}_2(R)$, respectively.

An important isotope effect is evident in the behavior of the four $\boldsymbol{w}(R)$ potentials. Specifically, when the helium nuclei are identical, there is no u-g coupling, and so these terms contribute only to diagonal (uncoupled, adiabatic) energy corrections for the $U^u(R)$ and $U^g(R)$ potentials. However, when the nuclei are nonidentical, there is an off-diagonal

TABLE II. Comparison of experimental and theoretical values (cm^{-1}) of the $(v'=1,N') \leftarrow (v''=0,N'')$ transition energies of $^3He\,^4He^+$ in the electronic ground state.

		Theoretical					
N'-N''	Expt.	CR	CPK	CPK′	BO	Modified Born	Fully coupled
1-0		1766.454		1766.89	1765.718	1766.326	1766.326
2-1	1781.839	1781.808	1782.072	1783.04	1781.070	1781.689	1781.687
3-2		1796.559	1796.821	1797.52	1795.820	1796.448	1796.449
4-3	1810.717	1810.692	1810.951	1811.69	1809.954	1810.591	1810.593
5-4	1824.212	1824.190	1824.498	1825.23	1823.454	1824.102	1824.101
6-5	1837.055	1837.035	1837.287	1838.09	1826.293	1836.965	1836.970
7-6	1849.719	1849.212	1849.460	1850.33	1848.485	1849.158	1849.153
8-7	1860.229	1860.701	1860.948	1861.85	1859.984	1860.668	1860.670
9-8		1871.494	1871.733	1871.85	1870.782	1871.475	1871.476
10-9	1881.580	1881.566	1881.801	1882.76	1880.865	1881.572	1881.573
11-10	1890.916	1890.906	1891.135	1892.15	1890.217	1890.932	1890.931
12-11	1899.509	1899.496	1899.720	1900.78	1898.821	1899.551	1899.549
rms		0.018	0.227	1.064	0.737	0.088	0.087

u-g coupling contribution. Indeed, it is exactly these off-diagonal terms that allow the electron transfer reactions

$$^4He^+ + {}^3He \leftrightarrows {}^4He + {}^3He^+ \tag{18}$$

to proceed.

The numerical calculation of each of the four $\boldsymbol{w}(R)$ terms, and the development of analytical expressions for fitting the general R dependence of these functions, will now be considered. The analytic functional forms used were dictated by the shape of the curves, rather than by any theoretically based criterion. Unless stated otherwise, the bra and ket notation in the following sections indicates integration over all electron coordinates, in the nuclear center-of-mass (c.m.) frame. The atomic mass of ^3He and ^4He are 3.016 029 31 and 4.002 603 250 amu, respectively.[35] In the subsequent calculations, nuclear masses, taken to be the atomic mass minus the mass of two electrons, were used.

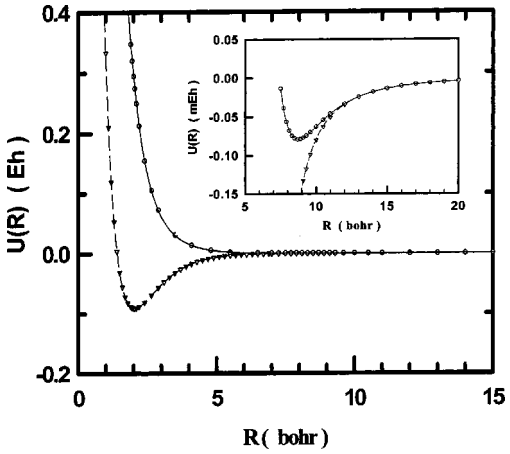

FIG. 1. Plot of the Born–Oppenheimer potentials for the ground $X^2\Sigma_u^+$ (triangles) and first-excited $A^2\Sigma_g^+$ (circles) electronic states of He_2^+. The curves represent the analytical functions fit to these potentials following Eqs. (11) and (12), respectively. The inset plot shows the shallow well present in the $A^2\Sigma_g^+$ potential.

1. Mass polarization

The mass polarization matrix elements are given by

$$w_{\rm mp}^{nm}(R) = \langle \Phi_e^n(r;R) | \hat{\boldsymbol{T}}_{\rm mp} | \Phi_e^m(r;R) \rangle. \tag{19}$$

$\hat{\boldsymbol{T}}_{\rm mp}$ is given by Eq. (6), from which it is clear that the mass polarization may also be interpreted in terms of the total linear electron momentum, $\hat{P}^2 = \vec{\hat{P}} \cdot \vec{\hat{P}}$, via $\hat{\boldsymbol{T}}_{\rm mp} = -(\hbar^2/2M)\hat{P}^2$. This relation is useful, as it allows one to show that the off-diagonal coupling contribution, $w_{\rm mp}^{gu}(R)$, must be zero. This can be achieved using a simple symmetry argument, as follows. The appropriate symmetry group for $\hat{H}_e$ is $D_{\infty h}$. Because the magnitude of the momentum vector is unchanged under all symmetry operations of this group, the character of $\hat{\boldsymbol{T}}_{\rm mp}$ must be Σ_g^+. Therefore, $w_{\rm mp}^{nm}(R)$ is nonzero if and only if $\Sigma_n^+ \otimes \Sigma_g^+ \otimes \Sigma_m^+ = \Sigma_g^+$. This is the case for $n=m=u$ and for $n=m=g$, but not for the off-diagonal g-u case.

For computing the diagonal corrections, $w_{\rm mp}^{nn}(R)$, it is convenient to decompose $\hat{\boldsymbol{T}}_{\rm mp}$ into a sum of one ($\hat{\boldsymbol{T}}_{\rm mp_1}$) and two ($\hat{\boldsymbol{T}}_{\rm mp_2}$) electron operators, given by

$$\hat{\boldsymbol{T}}_{\rm mp_1} = -\frac{\hbar^2}{2M}\sum_{i=1}^{3} \nabla_i^2, \tag{20}$$

$$\hat{\boldsymbol{T}}_{\rm mp_2} = -\frac{\hbar^2}{2M}\sum_{i\neq j} \nabla_i \cdot \nabla_j. \tag{21}$$

$\hat{\boldsymbol{T}}_{\rm mp_1}$ is proportional to the total electron kinetic energy and its contribution to $w_{\rm mp}^{nn}(R)$ can be readily evaluated using standard capabilities of MOLPRO2003.3.

In contrast, exact evaluation of the $\hat{\boldsymbol{T}}_{\rm mp_2}$ contribution is not a standard feature supported by MOLPRO or any other electronic structure package of which we are aware. To evaluate these matrix elements, we exploited the resolution of the identity by inserting a sum over electronic states in the middle of Eq. (21):

$$\hat{T}_{\mathrm{mp}_2} = -\frac{\hbar^2}{2M}\sum_k \sum_{i\neq j} \nabla_i |\Phi_e^k\rangle \cdot \langle \Phi_e^k| \nabla_j. \tag{22}$$

This expression was then sandwiched in between the bra and ket vectors, $\langle \Phi_e^n|$ and $|\Phi_e^n\rangle$, in order to obtain the desired matrix elements $w_{\mathrm{mp}_2}^{nn}$. The numerical sum over intermediate states Φ_e^k was performed in order of increasing energy and truncated when convergence was achieved.

Note that although the indices n and m range only over the two electronic states of interest ($X\,^2\Sigma_u^+$ and $A\,^2\Sigma_g^+$), k spans a much broader range of intermediate electronic states. Moreover, the accurate evaluation of Eq. (22) requires a high quality description of these intermediate states, which in turn requires a more extensively diffuse basis set to accommodate the increased spatial extent of the excited electronic states. For these calculations, the cc-pV5Z basis set[25] augmented with a (5*s*5*p*5*d*4*f*3*g*) set of uncontracted diffuse functions[25] was used. The quality of this basis set was assessed by comparing the calculated properties of excited electronic states of He, He_2^+, and He_2 with available theoretical and experimental informations. The MRCISD calculations with this more extensive basis set were found to accurately describe all He atomic electronic states up to principle quantum number $n=3$ and all of the molecular states dissociating to these levels. The detailed results of these calculations will be presented elsewhere.

The matrix elements $w_{\mathrm{mp}_2}^{nn}$ as obtained from the Eq. (22) summation are easily expressed in terms of the matrix elements for the electron velocity operator, which in turn are readily obtained using the standard capabilities of MOLPRO2003.3. To test the validity of this approach, we first applied the technique to a single helium atom. The one- and two-electron contributions to $\boldsymbol{w}_{\mathrm{mp}}$ for the ground state of ^{4}He were calculated to be 87.31 cm^{-1} and -4.76 cm^{-1}, respectively. These results agree very well with the high-level calculations of Pekeris[17] who reported 87.33 cm^{-1} and -4.79 cm^{-1} for the corresponding values.

As we are interested in considering different isotopic variants, it is convenient to work with the nuclear mass-independent quantity, $Mw_{\mathrm{mp}}(R)$. This enables us to develop analytical curve-fitting expressions valid for all isotope combinations. The calculated results for the diagonal one-electron contributions, $Mw_{\mathrm{mp}_1}^{uu}$ and $Mw_{\mathrm{mp}_1}^{gg}$, are shown in Fig. 2. The R dependence of these quantities was fit using the expressions

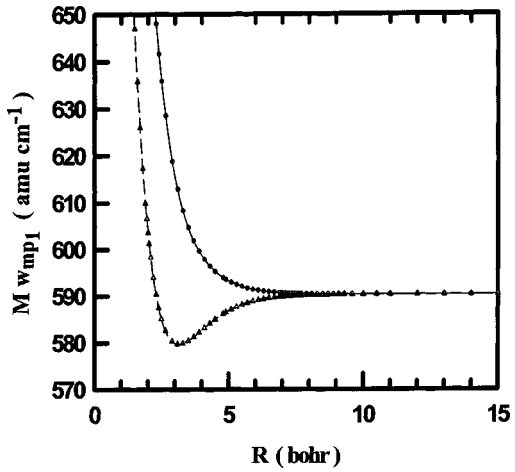

FIG. 2. Plot of the diagonal one-electron mass polarization matrix elements, $Mw_{mp_1}^{uu}(R)$ (triangles) and $Mw_{mp_1}^{gg}(R)$ (circles), for He_2^+ as a function of nuclear separation R. The curves represent the analytical functions fit to these matrix elements following Eqs. (23) and (24), respectively.

$$Mw_{\mathrm{mp}_1}^{uu}(R) = \sum_{k=0}^{3} a_k (R-R_0)^k e^{b(R-R_0)} + d, \tag{23}$$

$$Mw_{\mathrm{mp}_1}^{gg}(R) = b_0 e^{-b_1 R} + s_s(R)\sum_{k=0}^{3} a_k (R-R_0)^k e^{b(R-R_0)} + d. \tag{24}$$

Values for the optimized parameters in Eqs. (23) and (24) are given in Table III of the associated EPAPS material.[34] These resulted in rms errors of 0.059 amu cm^{-1} and 0.143 amu cm^{-1}, and maximum errors of -0.107 amu cm^{-1} occurring at 1.5 bohrs and 0.218 amu cm^{-1} occurring at 2.04 bohrs for $Mw_{\mathrm{mp}_1}^{uu}$ and $Mw_{\mathrm{mp}_1}^{gg}$, respectively.

The computed two-electron results, for $Mw_{\mathrm{mp}_2}^{uu}$ and $Mw_{\mathrm{mp}_2}^{gg}$, are shown in Fig. 3, with the R dependence of these quantities modeled by the expressions

TABLE III. Comparison of experimental and theoretical values (cm^{-1}) for the $(A\,^2\Sigma_u^+, v', N') \leftrightarrow (X\,^2\Sigma_g^+, v'', N'')$ of $^4He_2^+$.

		Theoretical			
v', N'-v'', N''	Expt.	CPK	CPK′	BO	Modified Born
23,3-1,2	0.298	0.243	0.300	0.264	0.276
23,1-1,0	1.655	0.559	1.650	1.594	1.627
23,3-0,4	1.863	1.917	1.860	1.914	1.920
23,1-1,2	2.298	2.198	2.290	2.234	2.270
22,5-0.4	3.383	3.031	3.380	3.439	3.450
23,1-0,2	3.819	3.914	3.820	3.903	3.885
23,1-0,0	5.625	5.718	5.630	5.711	5.690
rms		0.154	0.004	0.064	0.051

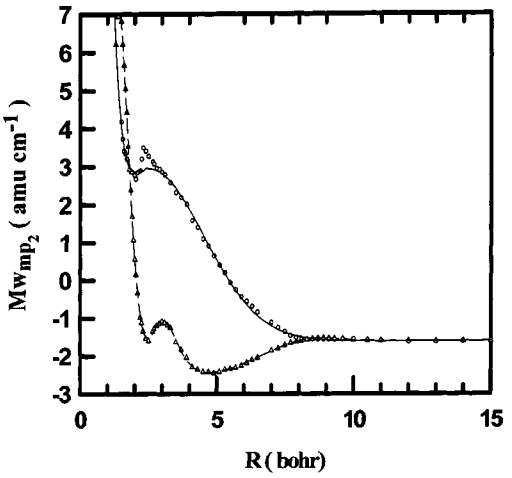

FIG. 3. Plot of the diagonal two-electron mass polarization matrix elements, $Mw^{uu}_{mp_2}(R)$ (triangles) and $Mw^{gg}_{mp_2}(R)$ (circles), for He_2^+ as a function of nuclear separation R. The curves represent the analytical functions fit to these matrix elements following Eqs. (25) and (26), respectively.

$$Mw^{uu}_{\mathrm{mp}_2}(R) = r_0\frac{r_1^2}{(R-r_2)^2+r_1^2} + c_0\{1+\tanh[c_1(R-c_2)]\} + b_0e^{-(b_1R+b_2R^2)} + g_0e^{-[(R-g_2)/g_1]} + d, \quad (25)$$

$$Mw^{gg}_{\mathrm{mp}_2}(R) = r_0\frac{r_1^2}{(R-r_2)^2+r_1^2} + b_0e^{-(b_1R+b_2R^2)} + b_0'e^{-(b_1'R+b_2'R^2)} + d. \quad (26)$$

Values for the optimized parameters in Eqs. (25) and (26) that resulted in a rms errors of 0.032 amu cm^{-1} and 0.077 amu cm^{-1}, and maximum errors of −0.106 amu cm^{-1} occurring at 1.65 bohrs and −0.116 amu cm^{-1} occurring at 2.04 bohrs for $Mw^{uu}_{\mathrm{mp}_2}$ and $Mw^{gg}_{\mathrm{mp}_2}$, respectively, are given in Table IV of the associated EPAPS material.[34]

As explained earlier, the off-diagonal terms should vanish for both one-electron and two-electron matrix elements. As a check on the overall accuracy of the numerical method, however, we performed numerical calculations for these terms. The results were identically zero, except for the $Mw^{gu}_{\mathrm{mp}_2}$ calculation for isotopically distinguishable nuclei. The calculated magnitude of the latter for $^3He\,^4He^+$ was never greater than 2×10^{-3} amu cm^{-1}, which is well below our accuracy threshold.

2. Electron orbital angular momentum

The BOC electron orbital angular momentum matrix elements are given by

$$w_l^{nm}(R) = \frac{1}{2\mu R^2}\langle\Phi_e^n(r;R)|\hat{\boldsymbol{L}}^2|\Phi_e^m(r;R)\rangle. \quad (27)$$

A subtlety arises from the fact that $\hat{\boldsymbol{L}}^2$ refers to the nuclear c.m. origin [i.e., the last term of Eq. (5)], whereas the symmetry of the electronic states is with respect to the nuclear center of charge (CC) origin, i.e., $(\vec{R}_A'+\vec{R}_B')/2$. These two origins are identical for homonuclear isotopologs, but different for heteronuclear isotopologs.

To develop a single description that works for both cases, it is convenient to transform Eq. (27) to the CC frame. This is achieved via the electronic coordinate transformation,

$$x_i = x_i^{\mathrm{CC}}, \quad y_i = y_i^{\mathrm{CC}}, \quad z_i = z_i^{\mathrm{CC}} - \delta R, \quad \delta = \left[\frac{m_B - m_A}{2M}\right], \quad (28)$$

where δ is the mass difference ratio, which distinguishes different isotopologs. Equation (28) gives rise to

$$\vec{\hat{L}} = \vec{\hat{L}}_{\mathrm{CC}} - \delta\vec{R}\times\vec{\hat{P}}, \quad (29)$$

which in turn yields the following expression for $\hat{L}^2$:

$$\hat{\boldsymbol{L}}^2 = \hat{\boldsymbol{L}}^2_{\mathrm{CC}} + \delta R(\hat{\boldsymbol{L}}_x^{\mathrm{CC}}\hat{\boldsymbol{P}}_y + \hat{\boldsymbol{P}}_y\hat{\boldsymbol{L}}_x^{\mathrm{CC}} - \hat{\boldsymbol{L}}_y^{\mathrm{CC}}\hat{\boldsymbol{P}}_x - \hat{\boldsymbol{P}}_x\hat{\boldsymbol{L}}_y^{\mathrm{CC}}) + \delta^2R^2(\hat{\boldsymbol{P}}_x^2 + \hat{\boldsymbol{P}}_y^2). \quad (30)$$

Equation (30) may be regarded as an (exact) expansion in δ, which is presumed small. For homonuclear isotopologs, $\delta=0$, and so only the first RHS term survives, i.e., $\hat{\boldsymbol{L}}^2=\hat{\boldsymbol{L}}^2_{\mathrm{CC}}$, as expected. For heteronuclear isotopologs, all three RHS terms must be retained; however, many of the resultant matrix elements are zero. This can once again be shown using symmetry arguments and by exploiting the fact that all quantities in Eq. (30) are now referred to the CC frame, as is

TABLE IV. Energy of the bound rovibrational levels of the $A\,^2\Sigma_g^+$ state of He_2^+ with respect to the dissociation limit.

	$^4He\,^4He^+$		$^3He\,^4He^+$		$^3He\,^3He^+$	
v,N	BO	Modified Born	BO	Modified Born	BO	Modified Born
0, 0	−8.0944	−8.1182	−7.5410	−8.9742	−7.0394	−7.0702
1, 0	−0.7895	−0.7997	−0.5247	−0.6652	−0.3395	−0.3486
2, 0	−0.0003	−0.0005				
0, 1	(−7.4854)	(−7.5096)	−6.8505	−8.2429	−6.2702	−6.3016
1, 1	(−0.5568)	(−0.5664)	−0.3022	−0.4174	−0.1361	−0.1436
0, 2	−6.2867	−6.3117	−5.4972	−6.8040	−4.7702	−4.8025
1, 2	−0.1489	−0.1568		−0.0073		
0, 3	(−4.5410)	(−4.5668)	−8.5441	−4.7105	−2.6295	−2.6625
0, 4	−2.3264	−2.3528	−1.1159	−2.0631	−0.0504	

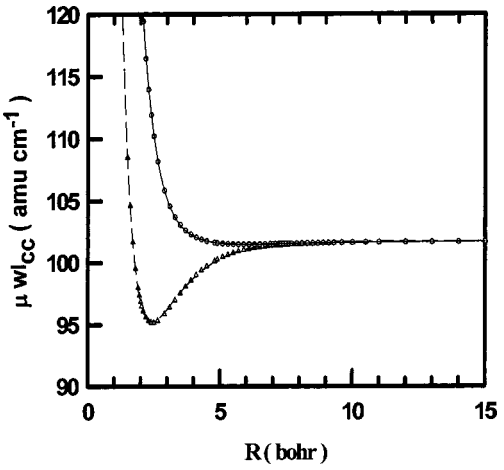

FIG. 4. Plot of the diagonal electronic angular momentum matrix elements, $\mu w_{l_\infty}^{uu}(R)$ (triangles) and $\mu w_{l_\infty}^{gg}(R)$ (circles), for He_2^+ as a function of nuclear separation R. The curves represent the analytical functions fit to these matrix elements following Eqs. (31) and (32), respectively.

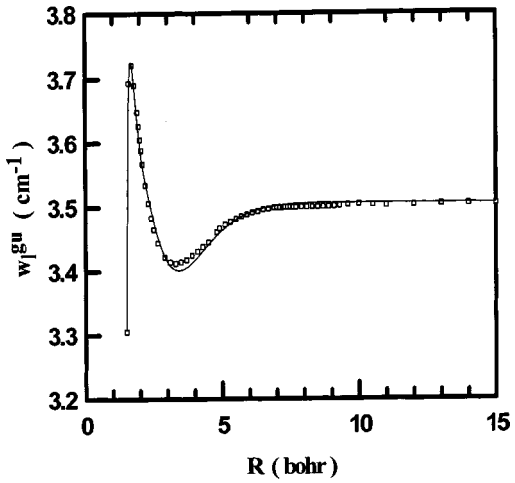

FIG. 5. Plot of the off-diagonal electronic angular momentum matrix element $w_l^{gu}(R)$ for $^3He\,^4He^+$ as a function of nuclear separation R. The curve represents the analytical functions fit to this matrix element following Eq. (33).

appropriate for the $\hat{H}_e$ symmetry group [the total linear electron momentum is unaffected by the coordinate change of Eq. (28)].

Using group theory arguments, it can be shown that the three terms in Eq. (30) have respective characters Σ_g^+, Σ_u^+, and Σ_g^+. As per Sec. II C 1, this implies that the first and last RHS terms are nonzero only for the diagonal matrix elements, i.e., for w_l^{gg} and w_l^{uu}. In contrast, the middle term is nonzero only for the off-diagonal matrix elements, $w_l^{ug} = w_l^{gu}$. This actually constitutes the dominant contribution to the coupling for $^3He\,^4He^+$—which is quite remarkable given that, to the authors' best knowledge, it has not been computed previously.

The numerical analysis begins with the first RHS term of Eq. (30), giving rise to the diagonal matrix element contribution $w_{l_{CC}}^{nn}(R)$. This can be evaluated using the standard capabilities of MOLPRO2003.3. Once again, we multiply Eq. (27) by the appropriate mass (in this case the nuclear reduced mass μ) to obtain a quantity that is explicitly nuclear mass independent, and therefore applicable to all isotopologs. The calculated values for $\mu w_{l_{CC}}^{uu}(R)$ and $\mu w_{l_{CC}}^{gg}(R)$ are shown in Fig. 4, with the R dependence of these quantities modeled by the expressions

$$\mu w_{l_{CC}}^{uu}(R) = \sum_{i=0}^{3} a_i (R - R_0)^i e^{-b(R-R_0)} + d, \tag{31}$$

$$\mu w_{l_{CC}}^{gg}(R) = b_0 e^{-b_1 R} + \sum_{i=0}^{2} \frac{d_i}{R^{\delta_i}} + d. \tag{32}$$

Values for the optimized parameters in Eq. (31) and (32) that resulted in rms errors of 0.082 amu cm^{-1} and 0.017 amu cm^{-1}, and maximum errors of 0.098 amu cm^{-1} occurring at 2.9 bohrs and 0.048 amu cm^{-1} occurring at 1.7 bohrs for $\mu w_{l_{CC}}^{uu}(R)$ and $\mu w_{l_{CC}}^{gg}(R)$, respectively, are given in Table V of the associated EPAPS material.[34]

The second RHS term in Eq. (30) is only relevant for heteronuclear isotopologs, for which it constitutes the entire off-diagonal $w_l^{gu}(R)$ coupling. Because, in the present study, the only such case is $^3He\,^4He^+$, we computed $w_l^{gu}(R)$ for this case directly. The results are shown in Fig. 5. The fit for the R dependence was modeled using the functional form

$$w_l^{gu}(R) = r_0 \frac{r_1^2}{(R - r_2)^2 + r_1^2} + \sum_{i=0}^{3} a_i (R - R_0)^i e^{-b(R-R_0)} + d. \tag{33}$$

Values for the optimized parameters in Eq. (33), which resulted in a rms error of 0.007 cm^{-1} and a maximum error of 0.0213 cm^{-1} occurring at 1.7 bohrs, are given in Table VI of the associated EPAPS material.[34] The abrupt change in behavior of $w_l^{gu}(R)$ at short distance may be due to the increased contribution of additional excited state electron configurations to the $X\,^2\Sigma_u^+$ and $A\,^2\Sigma_g^+$ states that become increasingly important at short distance particularly for the $A\,^2\Sigma_g^+$ state.

The third term in Eq. (30) is also only relevant for heteronuclear isotopologs, for which it contributes only to the diagonal matrix elements. Note that this contribution is proportional to δ^2, which is quite small (e.g., around 0.02 for $^3He\,^4He^+$), especially in comparison to the first RHS term contribution. A discussion of the numerical evaluation of the third term matrix elements is deferred to Sec. II C 4, for reasons explained therein.

3. First derivative with respect to R

The last two BOC terms stem from the differential operator of $\hat{T}_{vib}$, which applies to both the nuclear and electronic portions of the rovibronic wave function. To obtain a version that applies to the nuclear portion only, we construct matrix elements by sandwiching $\hat{T}_{vib}$ between the electronic states. This yields

$$\langle \Phi_e^n(r;R)|\hat{\boldsymbol{T}}_{\rm vib}|\Phi_e^m(r;R)\rangle = \delta_{nm}\left[\frac{-\hbar^2}{2\mu}\right]\frac{d^2}{dR^2} + w_1^{nm}(R)\frac{d}{dR} + w_2^{nm}(R), \tag{34}$$

where all explicit differentials in Eq. (34) apply to the nuclear states only. The first RHS term in Eq. (34) is the kinetic energy used in the vibrational Schrödinger equation; this contribution does not couple different electronic states.

The second RHS term in Eq. (34) is the first R derivative contribution to the BOC. The quantity $w_1^{nm}(R)$ is given by

$$w_1^{nm}(R) = -\frac{\hbar^2}{\mu}\left\langle \Phi_e^n(r;R)\left|\frac{\partial}{\partial R}\right|\Phi_e^m(r;R)\right\rangle, \tag{35}$$

where the partial differential in Eq. (35) applies only to the electronic ket state. This partial derivative is taken with respect to fixed electron coordinates in the c.m. frame. For symmetry reasons, it is convenient to express the partial differential in the CC frame. The result is

$$\frac{\partial}{\partial R} = \left[\frac{\partial}{\partial R}\right]_{\rm CC} + \delta\left[\frac{i}{\hbar}\right]\hat{\boldsymbol{P}}_z. \tag{36}$$

The characters of the two RHS terms in Eq. (36) are found to be Σ_g^+ and Σ_u^+, respectively. Thus, the first RHS term can be nonzero only for the diagonal matrix elements and the last RHS term can be nonzero only for the off-diagonal elements. On the other hand, it is well known that the diagonal matrix elements for the first R derivative contribution, i.e., the $w_1^{nn}(R)$, must be zero.[22] Consequently, for homonuclear isotopologs, *all* $w_1^{nm}(R)$ *matrix elements vanish*. For heteronuclear isotopologs, only the off-diagonal matrix elements $w_1^{gu}(R)$ are nonzero, and these can be easily obtained from the matrix elements for $\hat{\boldsymbol{P}}_z$.

For historical reasons, $w_1^{gu}(R)$ for the ^{3}He ^{4}He$^+$ isotopolog was not computed as described above, but using the following numerical scheme. Equation (35) was evaluated numerically using the central difference formula

$$w_1^{nm}(R) = {\rm Tr}(\gamma_{nm}^R S_{nm})/N_e + {\rm Tr}(\gamma_{nm}S_{nm}^R) + {\rm Tr}(\gamma_{nm}S_{nm}V_n^R V_m^T S_{mn}), \tag{37}$$

where Tr denotes the trace of the matrix, N_e is the number of electrons, γ_{nm} is the transition density between states n and m, S is the overlap matrix in the atomic orbital basis, and V is the molecular orbital eigenvector. In Eq. (37), the superscript R denotes numerical differentiation with respect to R according to

$$\gamma_{nm}^R(R) = [\langle \Phi_e^0(r;R)|\hat{\boldsymbol{E}}_{nm}|\Phi_e^0(r;R+\Delta)\rangle - \langle \Phi_e^0(r;R)|\hat{\boldsymbol{E}}_{nm}|\Phi_e^0(r;R-\Delta)\rangle]/2\Delta, \tag{38}$$

$$S_{nm}^R(R) = [\langle \Phi_e^n(r;R)|\Phi_e^m(r;R+\Delta)\rangle - \langle \Phi_e^n(r;R)|\Phi_e^m(r;R-\Delta)/2\Delta, \tag{39}$$

$$V_n^R(R) = [V_n(R+\Delta) - V_n(R-\Delta)]/2\Delta, \tag{40}$$

where $\hat{\boldsymbol{E}}_{nm}$ is the one-particle excitation operator. The value of Δ was varied to ensure convergence to about 0.1% and typically had values of about 0.01 bohr near the minimum of the $X\,^2\Sigma_u^+$ curve and about 0.05 bohr at longer distances.

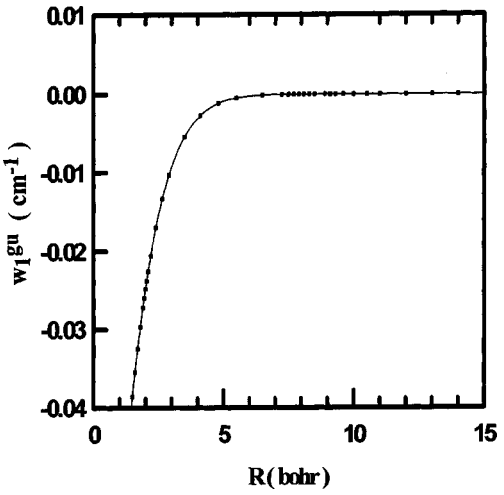

FIG. 6. Plot of the off-diagonal first R derivative matrix element $w_1^{gu}(R)$ for ^{3}He^{4}He$^+$ as a function of nuclear separation R. The curve represents the analytical function fit to this matrix element following Eq. (41).

Computed values for $w_1^{gu}(R)$ for ^{3}He ^{4}He$^+$ are shown in Fig. 6 with the R dependence modeled by

$$w_1^{gu}(R) = -b_0 e^{-(b_1 R + b_2 R^2)} + S_l(R)\frac{c}{R^\delta}. \tag{41}$$

Values for the optimized parameters in Eq. (47), which resulted in rms error of 1.7×10^{-5} cm^{-1} and a maximum error of -0.429 cm^{-1} occurring at 1.65 bohrs for $w_1^{gu}(R)$, are given in Table VII of the associated EPAPS material.[34]

4. Second derivative with respect to R

The second R derivative contribution to the BOC is given by

$$w_2^{nm}(R) = -\frac{\hbar^2}{2\mu}\left\langle \Phi_e^n(r;R)\left|\frac{\partial^2}{\partial R^2}\right|\Phi_e^m(r;R)\right\rangle. \tag{42}$$

Transforming the partial differential operator to the CC frame yields

$$\frac{\partial^2}{\partial R^2} = \left[\frac{\partial^2}{\partial R^2}\right]_{\rm CC} + 2\delta\left[\frac{\partial}{\partial R}\right]_{\rm CC}\left[\frac{i}{\hbar}\right]\hat{\boldsymbol{P}}_z - \delta^2\left[\frac{1}{\hbar^2}\right]\hat{\boldsymbol{P}}_z^2. \tag{43}$$

The characters of the three terms in Eq. (43) are Σ_g^+, Σ_u^+, and Σ_g^+, respectively. Thus, the first and last terms are nonzero only for the diagonal matrix elements, and the middle term is nonzero only for the off-diagonal elements.

Equation (43) makes it clear that, as with the other BOCs, only the heteronuclear isotopolog ^{3}He ^{4}He$^+$ yields coupling between the two electronic states. Moreover, the magnitude is on the same order as that of the electron orbital angular momentum contribution of Sec. II C 2. The same can be said of the diagonal, order δ^2 contribution of Eq. (43), and the corresponding electron orbital angular momentum term in Eq. (30). Indeed, by combining the latter two together, we find that the total order δ^2 contribution is just

$$O(\delta^2) = \delta^2 \left[\frac{M}{\mu} \right] \hat{\boldsymbol{T}}_{\mathrm{mp}}. \tag{44}$$

Accordingly, the most effective way to compute these matrix elements numerically is directly in terms of the mass polarization matrix elements, as per Sec. II C 1.

The second R derivative matrix elements were computed using a method analogous to that of Sec. II C 3. It is convenient to express $w_2^{nm}(R)$ as the sum of a one-electron term $w_{2_1}^{nm}(R)$ and a two-electron term $w_{2_2}^{nm}(R)$ given by

$$\begin{aligned} w_{2_1}^{nm}(R) = {} & \mathrm{Tr}(\gamma_{nm}^{RR} S_{nm})/N_a + \mathrm{Tr}(\gamma_{nm} S^{RR}) \\ & + \mathrm{Tr}(S_{nm} V_n^{RR} V_m^T S_{mn}) + 2\,\mathrm{Tr}(\gamma_{nm}^R S_{nm}^R) \\ & + 2\,\mathrm{Tr}(\gamma_{nm}^R S_{nm} V_n^R V_m^T S_{mn}) \\ & + 2\,\mathrm{Tr}(\gamma_{nm} S_{nm}^R V_n^R V_m S_{mn}), \end{aligned} \tag{45}$$

$$w_{2_2}^{nm}(R) = \sum_{ij,kl} \delta_{ij,kl}^{nm(2)} M_{ij}^R M_{kl}^R. \tag{46}$$

In Eq. (45), the superscript RR denotes double numerical differentiation with respect to R, according to

$$\begin{aligned} \gamma_{nm}^{RR}(R) = {} & [\langle \Phi_e^0(r;R) | \hat{\boldsymbol{E}}_{nm} | \Phi_e^0(r;R+\Delta) \rangle \\ & + \langle \Phi_e^0(r;R) | \hat{\boldsymbol{E}}_{nm} | \Phi_e^0(r;R-\Delta) \rangle] \\ & - 2\langle \Phi_e^0(r;R) | \hat{\boldsymbol{E}}_{nm} | \Phi_e^0(r;R) \rangle / 2\Delta, \end{aligned} \tag{47}$$

$$\begin{aligned} S_{nm}^{RR}(R) = {} & [\langle \Phi_e^n(r;R) | \Phi_e^m(r;R+\Delta) \rangle \\ & + \langle \Phi_e^n(r;R) | \Phi_e^m(r;R-\Delta) \\ & - 2\langle \Phi_e^n(r;R) | \Phi_e^m(r;R) \rangle / 2\Delta, \end{aligned} \tag{48}$$

$$V_n^{RR}(R) = [V_n(R+\Delta) + V_n(R-\Delta) - 2V_n(R)]/2\Delta. \tag{49}$$

In Eq. (46), $\delta_{ij,kl}^{nm(2)}$ is the two-electron density matrix and the matrix $M_{\alpha\beta}^R$ is given by

$$M_{\alpha\beta}^R = V^T S^R V + V^T S V^R. \tag{50}$$

The diagonal matrix elements were computed in the CC frame, giving rise to the first RHS term contribution from Eq. (43). Results for $\mu w_{2_{\mathrm{CC}}}^{uu}(R)$ and $\mu w_{2_{\mathrm{CC}}}^{gg}(R)$ are shown in Fig. 7 with the R dependence modeled by

$$\begin{aligned} \mu w_{2_{\mathrm{CC}}}^{uu}(R) = {} & \sum_{i=0}^{3} a_i (R - R_0)^i e^{-b(R-R_0)} + b_0 e^{-b_1 R} \\ & + c_l s_l(R) + d, \end{aligned} \tag{51}$$

$$\mu w_{2_{cc}}^{gg}(R) = \sum_{i=0}^{3} a_i (R - R_0)^i e^{-b(R-R_0)} + d. \tag{52}$$

Values for the optimized parameters in Eqs. (51) and (52), which resulted in rms errors of 0.032 amu cm^{-1} and 0.077 amu cm^{-1} and maximum errors of 1.123 amu cm^{-1} occurring at 1.6 bohrs and 1.142 amu cm^{-1} occurring at 1.7 bohrs, for $\mu w_{2_{\mathrm{CC}}}^{uu}(R)$ and $\mu w_{2_{cc}}^{gg}(R)$, respectively, are given in Table VIII of the associated EPAPS material.[34]

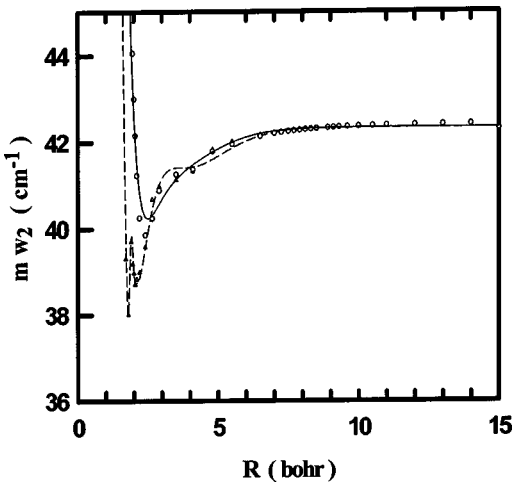

FIG. 7. Plot of the diagonal second R derivative matrix elements, $\mu w_{2\alpha}^{uu}(R)$ and $\mu w_{2\alpha}^{gg}(R)$, for He_2^+ as a function of nuclear separation R. The curves represent the analytical functions fit to these matrix elements following Eqs. (51) and (52), respectively.

The off-diagonal matrix elements, i.e., $w_2^{gu}(R)$ for $^3He\,^4He^+$, were computed in the c.m. frame. Results are presented in Fig. 8 with the R dependence modeled by

$$w_2^{gu}(R) = \sum_{i=0}^{1} r_{i0} \frac{r_{i1}}{(R - r_{i2})^2 + r_{i1}^2} + d \quad \text{for } R \leqslant r_{i2}, \tag{53}$$

$$\begin{aligned} w_2^{gu}(R) = {} & \sum_{i=0}^{1} g_{i0} e^{-[(R - g_{i2})/g_{i1}]^2} \\ & + \sum_{i=1}^{2} \frac{r_{i1}}{(R - r_{i2})^2 + r_{i1}^2} + d \quad \text{for } R \geqslant r_{i2}. \end{aligned} \tag{54}$$

Values for the optimized parameters in Eqs. (53) and (54), which resulted in a rms error of 0.061 cm^{-1} and a maximum error of 0.145 cm^{-1} for $w_2^{gu}(R)$ occurring at 2.1 bohrs, are given in Table IX of the associated EPAPS material.[34] The cause of the sharp peaks near 2 bohrs and 9 bohrs is not clear, although at the shorter distance there may be increased

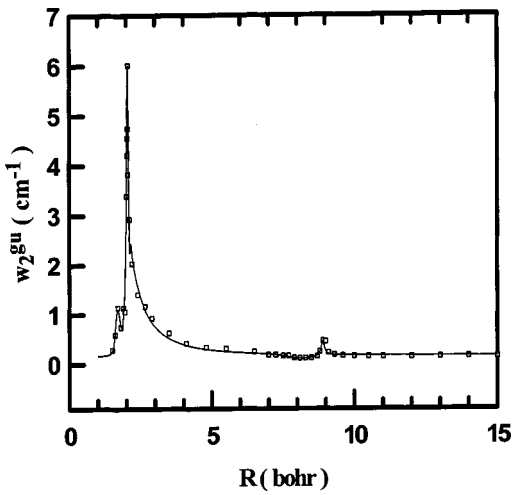

FIG. 8. Plot of the off-diagonal second R derivative matrix element $w_2^{gu}(R)$ for $^3He^4He^+$ as a function of nuclear separation R. The curve represents the analytical function fit to this matrix element following Eqs. (53) and (54).

excited electronic state contributions similar to that suggested in the context of $w_l^{gu}(R)$. However, such contributions are not expected to be important near 9 bohrs, a distance near the $A\,^2\Sigma_g^+$ state energetic minima. Nevertheless, the peaks do not appear to be the result of a computational or numerical artifact.

The calculated data represented in Figs. 1–8 are given in Tables X–XII of the associated EPAPS material.[34]

D. Asymptotic Born–Oppenheimer correction energy

At $R=\infty$, the BOC energy can be calculated in either an atomic or a molecular framework. In an atomic framework, mass polarization accounts for the entire BOC, whereas in a molecular framework, the effect is divided among the mass polarization, electronic angular momentum, and the second R derivative terms. Thus, a comparison between results calculated in the two frameworks provides a check on the internal consistency of the calculations. Furthermore, the BOC for a homonuclear isotopolog isolates the diagonal contribution, whereas the BOC-induced energy separation of the ^{4}He $+\,^3$He$^+$ (lower energy) and ^{4}He$^+ + \,^3$He (higher energy) diabatic potential asymptotes isolates the off-diagonal BOC contribution.

For ^{4}He$+\,^4$He$^+$, a total BOC asymptotic energy of 142.702 cm^{-1} is determined in the atomic framework, which agrees extremely well with the 142.709 cm^{-1} calculated by Pekeris.[17] In the molecular framework, a comparable value of 144.132 cm^{-1} is calculated, for which the contributions from mass polarization, electronic angular momentum, and the second R derivative terms are 72.142 cm^{-1}, 50.834 cm^{-1}, and 21.156 cm^{-1}, respectively.

For the ^{4}He$+\,^3$He$^+$ and ^{4}He$^+ + \,^3$He asymptotic energy separation, a value of 7.329 cm^{-1} is determined in the atomic framework, which agrees very well with the 7.318 cm^{-1} calculated by Perkeris.[5] In the molecular framework, a comparable value of 7.304 cm^{-1} is calculated, for which the contributions from mass polarization, electronic angular momentum, and the second R derivative terms are 0.000 cm^{-1}, 7.010 cm^{-1}, and 0.294 cm^{-1}, respectively.

E. Bound state calculation

Using Eq. (9) and the previous sections, a compact matrix representation of the rovibronically coupled nuclear motion Schrödinger equations can be written as[5,6,36]

$$\left\{\left[\left(\frac{-\hbar^2}{2\mu}\right)\frac{d^2}{dR^2}+\frac{N(N+1)}{2\mu R^2}\right]\boldsymbol{I}+\varepsilon(R)+w_1(R)\frac{d}{dR}\right\}\chi(R) = E_\chi(R), \tag{55}$$

where $\varepsilon(R)$ is the BO-plus-BOC 2×2 effective potential matrix, given by

$$\varepsilon(R)=\boldsymbol{w}_{\rm mp}(R)+\boldsymbol{w}_l(R)+\boldsymbol{w}_2(R)+\boldsymbol{V}_e(R). \tag{56}$$

Setting $\boldsymbol{w}_{\rm mp}(R)=\boldsymbol{w}_l(R)=\boldsymbol{w}_1(R)=\boldsymbol{w}_2(R)=0$, recovers the BO approximation, and the resulting uncoupled, rovibration Schrödinger equations

$$\left\{\left[\left(\frac{-\hbar^2}{2\mu}\right)\frac{d^2}{dR^2}+\frac{N(N+1)}{2\mu R^2}\right]\boldsymbol{I}+\boldsymbol{V}_e(R)\right\}\chi_{\rm BO}(R) = E_{\rm BO}\chi_{\rm BO}(R). \tag{57}$$

Equation (57) was solved using the discrete variable representation (DVR) methodology,[37–46] representing $\chi_{\rm BO}(R)$ in a sinc-DVR basis. For $N=0$, the resultant BO energies $E_{\rm BO}$ and nuclear wave functions $\chi_{\rm BO}(R)$ serve as a convenient basis for solving Eq. (55). Before doing so, however, an adiabatic-to-diabatic (ATD) transformation was first performed to minimize the contribution of the $w_1(R)$ term to Eq. (55), because the d/dR operator can be difficult to deal with numerically. In the present two-state case, the transformation matrix $\boldsymbol{A}(R)$ is given by

$$\boldsymbol{A}(R)=\begin{pmatrix}\cos\beta & -\sin\beta\\ \sin\beta & \cos\beta\end{pmatrix}, \tag{58}$$

where β is given by

$$\beta(R)=\beta(\infty)+\left(\frac{\mu}{\hbar^2}\right)\int_R^\infty w_1^{\rm gu}(R)dR. \tag{59}$$

In the present application, this ATD transformation also has an important physical significance, in that coupling in the diabatic representation vanishes in the asymptotic dissociation limit of large nuclear separation R. Thus, whereas the adiabatic PESs become degenerate in the dissociation limit, this degeneracy is appropriately lifted for the diabatic PESs, giving rise to the asymptotic energy separation discussed in Sec. II D. The ATD transformed compact matrix coupled equation is given by

$$\left\{\left[\left(\frac{-\hbar^2}{2\mu}\right)\frac{d^2}{dR^2}+\frac{N(N+1)}{2\mu R^2}\right]\boldsymbol{I}+\varepsilon^d(R)\right\}\chi^d(R)=E\chi^d(R), \tag{60}$$

where $\varepsilon^d(R)$ and $\chi^d(R)$ are given by

$$\varepsilon^d(R)=\boldsymbol{A}(R)^\dagger\varepsilon(R)\boldsymbol{A}(R), \tag{61}$$

$$\chi^d(R)=\boldsymbol{A}(R)\chi(R). \tag{62}$$

Equation (60) was solved in two different ways. In the first approach, $\varepsilon^d(R)$ was diagonalized, resulting in uncoupled rovibration Schrödinger equations which were then solved separately. For homonuclear isotopologs, this is identical to the Born method. In the heteronuclear case, this approach is similar to the Born method, but yields "adiabatic" potentials with exact asymptotic behavior (i.e., the potentials are actually *diabatic* in the large R limit). We call this first approach the "modified Born" approach. In the second approach, the fully coupled, exact rovibronic equations were solved directly. We call this the "fully coupled" approach.

III. RESULTS

A. D_e and R_e

Values for the dissociation energy D_e and equilibrium bond length R_e for the ground $X\,^2\Sigma_u^+$ and first-excited $A\,^2\Sigma_g^+$ electronic states, calculated using the BO and modified Born

approaches, are compared to the previously computed BO results of CR and CPK, in Table I. Two BO potentials from the work of CPK were studied. The one denoted "CPK" resulted from high-level *ab initio* calculations. The one denoted "CPK′" resulted from an empirical scaling of the CPK potential, with the scale factor (1.001 28) chosen to maximize the agreement between theoretical and experimental values for the $(A\,^2\Sigma_g^+, v', N') \leftrightarrow (X\,^2\Sigma_u^+, v'', N'')$ electronic transitions of $^4He_2^+$.

For the ground electronic state, all of the BO results for R_e agree to within 10^{-3} a.u., and inclusion of the BOC terms increases R_e by about 0.6×10^{-3} a.u., independent of the isotopolog investigated. All of the BO results for the D_e of the ground state are also in substantial agreement with the present results, which agree with those of CR to within 0.16 cm^{-1} and with the unscaled results of CPK to within 2.5 cm^{-1}. However, the scaling procedure appears to somewhat degrade the ground state potential, with the D_e for the CPK′ potential being about 240 cm^{-1} larger than any of the nonscaled BO results. Inclusion of the BOC terms has little effect on the D_e for $^4He_2^+$ or $^3He_2^+$ ($\Delta D_e \leqslant 0.08$ cm^{-1}), but has a more substantial effect for $^3He\,^4He^+$ ($\Delta D_e = -4.8$ cm^{-1}).

For the D_e and R_e of the excited state, comparison can be made only to the CPK results. At the BO level, the present values of D_e and R_e agree with those of CPK to within 0.02 cm^{-1} and 8×10^{-3} a.u., respectively. Inclusion of the BOC terms has a much larger effect on the R_e of the excited state than it did for the ground state, with the R_e for $^4He_2^+$ and $^3He_2^+$ increasing by about 0.7×10^{-3} a.u. and 0.6×10^{-3} a.u., respectively, while the R_e for $^3He\,^4He^+$ decreases substantially by about 91×10^{-3} a.u. Similiarly, inclusion of BOCs has only a mild effect on the excited state D_e of the homonuclear isotopologs (increase of 0.037 cm^{-1} and 0.028 cm^{-1} for $^4He_2^+$ and $^3He_2^+$, respectively), but a substantially larger effect for $^3He\,^4He^+$ (increase of 2.996 cm^{-1}).

B. Rovibration spectra in the ground electronic state

Values for the $(v'=1, N') \leftarrow (v''=0, N'')$ infrared transitions of $^3He\,^4He^+$ in the ground electronic state $(X\,^2\Sigma_u^+)$ were calculated using the BO approximation, the modified Born approximation, and the exact, fully coupled treatment. These results are compared to experimental results, and to the previous BO-based calculations of CR and CPK, in Table II. Compared to the reported experimental values for nine transitions, the CPK and the present BO calculations have comparable agreement (rms errors of 0.227 cm^{-1} and 0.737 cm^{-1}, respectively) although the CPK results appear to be slightly superior. However, the empirical scaling factor present in the CPK′ potential degrades its ability to model these low-lying rovibration transitions (rms error = 1.064 cm^{-1}). For the present calculations, inclusion of the BOC terms dramatically increases the level of agreement with experiment by more than a factor of 8, with the modified Born and fully coupled treatments yielding nearly identical results (rms errors of 0.088 cm^{-1} and 0.087 cm^{-1}, respectively). Nevertheless, the BO results of CR, with no consideration of BOC effects, reproduce the experimental transition energies more faithfully (rms error = 0.018 cm^{-1}) than any other calculation to date.

C. Rovibronic transition spectra

Values for the rovibronic transitions observed for the $(A\,^2\Sigma_g^+, v', N') \leftrightarrow (X\,^2\Sigma_u^+, v'', N'')$ electronic band of $^4He_2^+$, as calculated in the BO and modified Born approximations, are compared to experimental results,[16] and to theoretical results obtained using the CPK and CPK′ BO potentials, in Table III. Inclusion of the BOC terms improves the agreement with experiment by about 20% (rms error deceases from 0.064 cm^{-1} to 0.051 cm^{-1}). However, this spectra is best modeled by the CPK′ potential (rms error = 0.004 cm^{-1}) which was adjusted specifically to agree with the experimental values. Without this adjustment (i.e., CPK potential), the agreement with experiment is substantially worse (rms error = 0.152 cm^{-1}).

D. Bound levels for the $A\,^2\Sigma_g^+$ state

For each of the naturally occurring isotopologs, there are no more than nine bound rovibration levels for the $A\,^2\Sigma_g^+$ electronic state, making it practical to report the energies for all of these levels. The binding energies of these levels calculated using the BO and modified Born approximations are reported in Table IV. The values in parentheses for $^4He_2^+$ represent levels which cannot be populated, because ^4He has a nuclear spin of zero, causing only even values of N to be populated in the $A\,^2\Sigma_g^+$ electronic state of this isotopolog. For the homonuclear isotopologs ($^4He_2^+$ and $^3He_2^+$), the effect of the BOCs on the energy levels is small, being generally less than 0.03 cm^{-1}. However, for the heteronuclear isotopolog ($^3He\,^4He^+$) this effect is substantially larger, decreasing the energy levels by as much as 1.5 cm^{-1}. It is interesting to note that the $(v, N) = (1, 2)$ level of $^3He\,^4He^+$ is predicted to be unbound in the BO approximation, but is predicted to be just barely bound in the modified Born approximation.

IV. DISCUSSION

The large well depth ($\sim$20 000 cm^{-1}) of the ground state potential significantly mitigates the effect of the relatively small BOCs on the D_e and R_e for this state. Although the excited state is much more weakly bound ($\sim$20 cm^{-1}), the magnitude of the BOC contribution is relatively independent of R for $R \geqslant \sim R_e$ causing them to have little effect on the values of D_e and R_e for the homonuclear isotopologs ($^4He_2^+$ and $^3He_2^+$). In contrast, the dramatic effect of the BOCs on the D_e and R_e for the $A\,^2\Sigma_g^+$ state of $^3He\,^4He^+$ can be seen as a direct consequence of the nonzero off-diagonal (in the adiabatic representation) contribution of the BOC terms in this case. In the asymptotic limit, these terms mix the degenerate ground and excited potentials, raising the energy of the excited state by about 3.65 cm^{-1} (i.e., half of the BOC asymptotic energy separation of about 7.30 cm^{-1}). Near the excited state R_e however, the two BO potentials are no longer degenerate, and their relatively large energy separation, as compared to the magnitude of the off-diagonal BOC

contribution, significantly diminishes the extent of PES mixing. Thus, D_e is increased by $\sim 3\ \mathrm{cm}^{-1}$, and R_e becomes shorter.

Although consideration of the BOC terms results in only a small change to the computed energies of the bound rovibration levels of He_2^+, the effect is not completely negligible. For the $v=0$ to $v=1$ vibrational transition of $^3He\,^4He^+$ in the $X\,^2\Sigma_u^+$ electronic state, the calculated transition energies are shifted upward by about 0.61–0.73 cm^{-1} with the magnitude of the shift increasing with N''. If these BOC energy shifts are applied to the BO results using CR, CPK, and CPK^{-1} potentials, and the resulting transition energies are compared with experiment, the resultant rms errors are 0.675 cm^{-1}, 0.883 cm^{-1}, and 1.806 cm^{-1}, respectively. These values are substantially larger than the rms values for the present BOC results (0.089 cm^{-1}). Indeed, the values are all substantially larger than the rms error for the corresponding BO potential. Thus, the agreement between the experimental results and the BO calculations of CR and CPK for these rovibrational transitions may be fortuitous.

The BOC adjustments to the energies of the observed rovibrational transitions in the $(A\,^2\Sigma_g^+, v', N') \leftrightarrow (X\,^2\Sigma_u^+, v'', N'')$ electronic band are more than an order of magnitude smaller than the BOC adjustments for the vibrational fundamental for the ground state. For this transition, application of the BOC energy shifts to the CPK BO results improves the agreement with experiment by about 8% (rms error decreases from 0.154 cm^{-1} to 0.142 cm^{-1}). Nevertheless, the present modified Born results more faithfully represent the observed spectra (rms error = 0.051 cm^{-1}). Of course, it is not sensible to apply a BOC adjustment to the CPK^{-1} results, as these employed a potential that was empirically adjusted to reproduce the transitions. Thus, the present, modified Born potentials for the $X\,^2\Sigma_u^+$ and $A\,^2\Sigma_g^+$ electronic states of He_2^+ provide the most accurate representations of both the low and high rovibrational levels of the ground state (i.e., $v=0$, 1, 22, 23) and the bound levels of the excited state currently available. Considering the quality of the experimental comparisons for the bound levels, it is expected that these potentials should be useful in accurately modeling He^+/He collision dynamics, particularly for processes, like reactions (1) or (18), that depend on the off-diagonal BOC terms.

ACKNOWLEDGMENTS

Grateful acknowledgment is made to the Robert A. Welch Foundation (Grant Nos. D-1293 and D-1523) for support of this work. Acknowledgment is also made to the Office of Advanced Scientific Computing Research, Mathematical, Information, and Computational Sciences Division of the U.S. Department of Energy under Contract No. DE-FG03-02ER25534.

[1] M. Born and J. R. Oppenheimer, Ann. Phys. **84**, 457 (1927).
[2] M. Born, Festschrift Gott. Nachr. Math. Phys. Kl. **1**, 1 (1951).
[3] M. Born and K. Huang, *Dynamical Theory of Crystal Lattices* (Oxford University Press, London, 1954).
[4] C. W. Kolos and L. Wolniewicz, Rev. Mod. Phys. **35**, 473 (1963).
[5] M. Baer, Adv. Chem. Phys. **124**, 39 (2002).
[6] A. Kupperman and R. Abrol, Adv. Chem. Phys. **124**, 283 (2002).
[7] J. M. Combes, Acta Phys. Austriaca, Suppl. **17**, 139 (1977).
[8] W. Cencek and J. Rychlewski, J. Chem. Phys. **102**, 2533 (1995).
[9] A. Carrington, C. H. Pyne, and P. J. Knowles, J. Chem. Phys. **102**, 5979 (1995).
[10] A. D. O. Bawagan and E. R. Davidson, Chem. Phys. Lett. **266**, 499 (1997).
[11] J. Ackermann and H. Hogrev, Chem. Phys. **157**, 75 (1991).
[12] C. W. Bauschlicher, Jr., H. Partridge, and D. Ceperley, Chem. Phys. Lett. **160**, 183 (1989).
[13] B. Liu, Phys. Rev. Lett. **27**, 1251 (1971).
[14] M. E. Schwartz and L. J. Schaad, J. Chem. Phys. **48**, 4709 (1968).
[15] P. N. Reagan, J. C. Browne, and F. A. Matsen, Phys. Rev. **132**, 304 (1963).
[16] N. Yu and W. H. Wing, Phys. Rev. Lett. **59**, 2055 (1987).
[17] C. L. Pekeris, Phys. Rev. **112**, 1649 (1958).
[18] G. I. Gellene, J. Phys. Chem. **97**, 34 (1993).
[19] J. Xie, B. Poirier, and G. I. Gellene, J. Chem. Phys. **119**, 10678 (2003).
[20] P. R. Bunker and P. Jensen, *Molecular Symmetry and Spectroscopy*, 2nd ed. (NRC Research Press, Ottawa, Ontario, Canada, 1998).
[21] L. C. Beidenharn and J. D. Louck, *Angular Momentum in Quantum Physics*, Encyclopedia of Mathematics and Its Applications Vol. 8 (Cambridge University Press, Cambridge, 1984).
[22] R. N. Zare, *Angular Momentum* (Wiley-Interscience, New York, 1998).
[23] J. H. van Vleck, Rev. Mod. Phys. **23**, 213 (1951).
[24] MOLPRO is a package of *ab initio* programs written by H.-J. Werner and P. J. Kmowles with contributions from J. Almlöf, R. D. Amos, M. J. O. Deegen *et al.*
[25] D. E. Woon and T. H. Dunning, Jr., J. Chem. Phys. **100**, 2975 (1994).
[26] H.-J. Werner and P. J. Knowles, J. Chem. Phys. **82**, 5053 (1985).
[27] P. J. Knowles and H.-J. Werner, Chem. Phys. Lett. **115**, 259 (1985).
[28] H.-J. Werner and E. A. Reinsch, J. Chem. Phys. **89**, 5803 (1988).
[29] P. J. Knowles and H.-J. Werner, Chem. Phys. Lett. **145**, 514 (1988).
[30] S. R. Langhoff and E. R. Davidson, Int. J. Quantum Chem. **8**, 61 (1974).
[31] D. M. Bishop and J. Pipen, Int. J. Quantum Chem. **45**, 349 (1993).
[32] D. M. Bishop and M. Rérat, J. Chem. Phys. **91**, 5489 (1989).
[33] W. D. Davidson, Proc. Phys. Soc. London **87**, 133 (1966).
[34] See EPAPS Document No. E-JCPSA6-122-303519 for Tables. A direct link to this document may be found in the online article's HTML reference section. The document may also be reached via the EPAPS homepage (http://www.aip.org/pubservs/epaps.html) or from ftp.aip.org in the directory /epaps/. See the EPAPS homepage for more information.
[35] G. Audi and A. H. Wapstra, Nucl. Phys. **A565**, 1 (1993).
[36] M. Baer, Phys. Rep. **358**, 75 (2002).
[37] D. T. Colbert and W. H. Miller, J. Chem. Phys. **96**, 1982 (1992).
[38] J. C. Light, I. P. Hamilton, and J. V. Lill, J. Chem. Phys. **82**, 1400 (1985).
[39] M. J. Bramley and T. Carrington, Jr., J. Chem. Phys. **99**, 8519 (1993).
[40] J. Echave and D. C. Clary, Chem. Phys. Lett. **190**, 225 (1992).
[41] J. C. Light and T. Carrington, Jr., Adv. Chem. Phys. **114**, 263 (2000).
[42] D. O. Harris, G. G. Engerholm, and W. D. Gwinn, J. Chem. Phys. **43**, 1515 (1965).
[43] Z. Bacic and J. C. Light, Annu. Rev. Phys. Chem. **40**, 469 (1989).
[44] R. G. Littlejohn, M. Cargo, T. Carrington, Jr., and B. Poirier, J. Chem. Phys. **116**, 8691 (2002).
[45] J. Montgomery and B. Poirier, J. Chem. Phys. **119**, 1 (2003).
[46] H. Wei and T. Carrington, Jr., J. Chem. Phys. **97**, 3029 (1992).